Journal of Solid State Chemistry **146,** 129–136 (1999)
Article ID jssc.1999.8318, available online at http://www.idealibrary.com on IDEAL®

Atomic Modeling of the $\delta \Leftrightarrow \varepsilon$ LiV_2O_5 Phase Transition and Simulation of the XRD Powder Pattern Evolution

Jean Galy,*,†,[1] Christine Satto,† Philippe Sciau,† and Patrice Millet†

*Institut für Anorganische Chemie, Auf der Morgenstelle 18, D-72076 Tübingen, Germany; and †Centre d'Elaboration de Matériaux et d'Etudes Structurales, du Centre National de la Recherche Scientifique, 29, rue Jeanne Marvig, BP 4347, 31055 Toulouse Cedex, France

Received January 20, 1999; in revised form March 25, 1999; accepted April 8, 1999

δ and ε LiV_2O_5 crystallize in the orthorhombic system, with *Cmcm* and *Pmmn* space groups, respectively. Transformation of δ into ε is initiated at about approximately 110°C. In both structures, lithium atoms are intercalated between $[V_2O_5]_n$ layers built up by VO_5 square pyramids sharing edges and corners, these layers being alternatively half shifted along the 3.6 Å parameter in the δ phase. Both crystal structures have been accurately depicted using $Pmn2_1$ space group with the short parameter along *c*. The phase transition, corresponding to a slip of $c/2$ of the alternate $[V_2O_5]_n$ layer of δ together with some lithiums, has been modeled step by step in order to be aligned along *c*, to finally match the ε structural organization. The shift vector *s* applied to *z* coordinates varies from $0 \le s \le 0.5$. The resulting evolution of the sequence of the computed X-ray powder pattern compares well with the experimental one done at ESRF ($\lambda = 0.64667$). The joint structural modeling and X-ray patterns account for the $\delta \Leftrightarrow \varepsilon$ LiV_2O_5 phase transition.

INTRODUCTION

In a recent paper, the study of the thermal behavior of the δ LiV_2O_5 using an X-ray powder diffraction line set up at the European Synchrotron Radiation Facility (ESRF), Grenoble, France, allowed us to specify clearly the remarkable series of phase transitions $\delta \Leftrightarrow \varepsilon \Rightarrow \gamma$ of this composition of the lithium–vanadium oxide bronzes (1).

The structural chemistry of the $Li_xV_2O_5$ system studied at 600°C was described by Galy *et al.* (2–4) as consisting of phases α, β, β', and γ LiV_2O_5 ($0 < x \le 1$). Then, new phases were isolated by soft chemistry at room temperature by Whittingham *et al.* (5), Murphy *et al.* (6), and Dickens *et al.* (7), i.e., α, ε, and δ LiV_2O_5. The α, ε, and δ structures (as well as β, β' and γ), feature a common parameter, $\sim$3.6 Å, along the double chains of $[VO_5]$ square pyramids sharing edges, these chains being connected by corners to form single layers, the second periodic length being approximately equal to 11.3 Å.

The α form could be roughly described as a low doping by lithium atoms in the layered structure of V_2O_5 ($x = 0.1$). The ε form exists for higher Li contents ($0.33 \le x \le 0.64$), with the α type structure, which is also the α' $Na_xV_2O_5$ one ($0.7 \le x \le 1$) (8). Lithium atoms occupy distorted bicapped triangular prisms between the $[V_2O_5]_n$ single layers. In fact, as demonstrated by Rozier *et al.* (9), using joint XRD and ^{6}Li, ^{7}Li MAS NMR techniques, the ε structure corresponds to two phases of limited solubility ranges $\varepsilon 1$ ($0.33 \le x \le 0.47$) and $\varepsilon 2$ ($0.53 \le x \le 0.63$) and a biphasic region $\varepsilon 1 + \varepsilon 2$ ($0.47 < x < 0.53$). In $\varepsilon 2$, the cell parameter *a*, which corresponds to the periodicity of the $[V_2O_5]_n$ layer (around 11.3 Å), markedly drops to $\varepsilon 1$ and causes a small distortion. $\varepsilon 1$ and $\varepsilon 2$ have incommensurate modulated structures (9, 10). $\varepsilon 1$ is described in the orthorhombic and $\varepsilon 2$ in the monoclinic systems.

The remaining δ $Li_xV_2O_5$ phase ($0.88 \le x \le 1$) crystallizes in the orthorhombic system with an original structure, as demonstrated by Cava *et al.* (11) in neutron powder diffraction experiments and more recently by Millet *et al.* (12) using X-ray data, together with the isostructural MgV_2O_5 compound.

This paper describes the modeling of atomic movements occurring during the $\delta \Leftrightarrow \varepsilon$ transition and the simulation of the continuous evolution of the corresponding X-ray powder patterns. As a result more insights are obtained at the atomic level into the experimental results provided by the ESRF experiment.

δ AND ε LiV_2O_5 STRUCTURES

These structures have already been described elsewhere (1, 11, 12) and are only briefly recalled. Orthorhombic δ and ε structures show a similar short parameter, i.e., $\sim$3.6 Å, the $[V_2O_5]_n$ layers being almost identical with a smooth variation of their μ puckering angles, 11.3° and 7.1°,

[1] To whom all correspondence should be addressed.

0022-4596/99 $30.00

respectively, along the longest parameter ~ 11.3 Å (δ: *Cmcm*, $a = 3.6047(2)$, $b = 9.9157(5)$, $c = 11.2479(4)$ Å at 21°C (12); ε: *Pmmn*, $a = 11.3552(6)$, $b = 3.5732(2)$, $c = 4.6548$ (3) Å at 140°C (1)).

A schematic of their projections along the short ~ 3.6 Å axis is shown in Fig. 1. The computed X-ray powder patterns for Cu$K\alpha$ radiation are plotted in Figs. 2a and 2b, for the δ and ε phases, respectively, using the structural data from Refs. (12) and (1). The parameters a and c of the δ phase have been permuted, while b and c of the ε phase were multiplied by 2.

When the amount of lithium atoms exceeds the bound limit of the $\varepsilon 2$ phase domain ($x > 0.64$) there exists a shift of $\sim 3.6/2$ Å of alternate layers in the direction of the shortest parameter, leading to a doubling of parameter b perpendicular to the $[V_2O_5]_n$ layers in the δ phase.

In the δ and ε phases, the lithiums exhibit a drastic variation of their oxygenated coordination polyhedra, CN $4+2$, as a bicapped tetrahedron in the former and CN $6+2$ as a bicapped triangular prism in the second.

$\delta \Leftrightarrow \varepsilon$ LiV_2O_5 PHASE TRANSITION

The $\delta \Leftrightarrow \varepsilon$ LiV_2O_5 phase transition occurs around 110°C and ends around 130°C and the irreversible $\varepsilon \Leftrightarrow \gamma$ LiV_2O_5 transformation is initiated at around 175°C, ending at 235°C (1). The $\delta \Leftrightarrow \varepsilon$ phase transition is reversible as shown by DSC measurements.

The shift of the $[V_2O_5]_n$ layers during formation of the δ phase, along the ~ 3.6 Å short axis, is obviously due to the "scratching" role of the inserted lithium atoms accompanying their intercalation process into the V_2O_5 layered structure. The increasing temperature reversibly promotes relaxation of the network with a readjustment of the $[V_2O_5]_n$ layers, i.e., reverse shift along the short axis, to yield the ε form.

ATOMIC MODELING OF THE $\delta \Leftrightarrow \varepsilon$ LiV_2O_5 PHASE TRANSITION

The first task consisted in describing the δ and ε crystal structures using the same space group. Then these preliminary assumptions were checked by computing their corresponding powder patterns and comparing them with those derived from previous structure analyses (Fig. 2) (1).

δ LiV_2O_5. This *Cmcm* crystal structure can be described with both space groups *Pmmn* or $Pmn2_1$. The $Pmn2_1$ (No. 31) space group was chosen because it allows the $[V_2O_5]_n$ layers as well as the lithium atoms to be described independently.

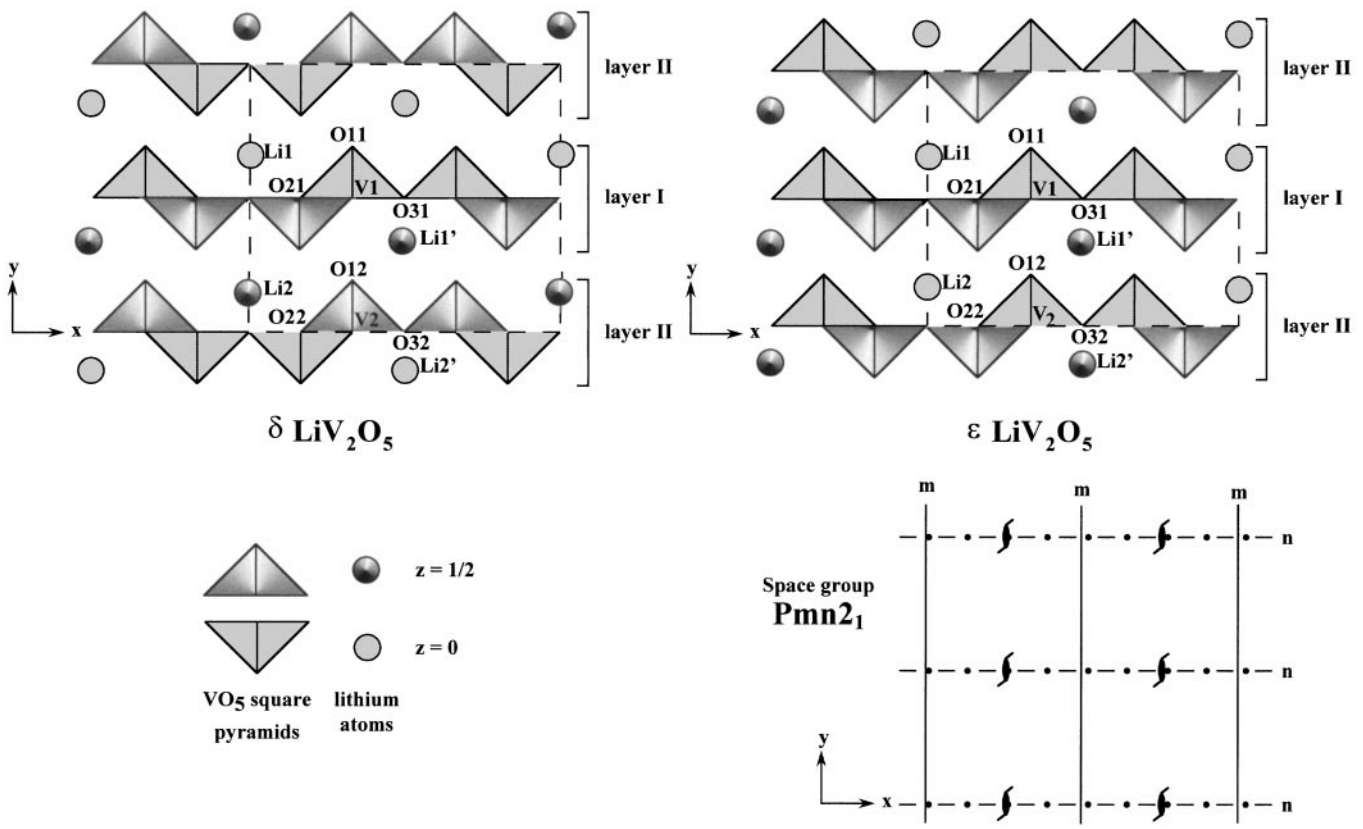

FIG. 1. Ideal projections of δ and ε LiV_2O_5 phases onto the (001) plane together with the plotting of the $Pmn2_1$ space group.

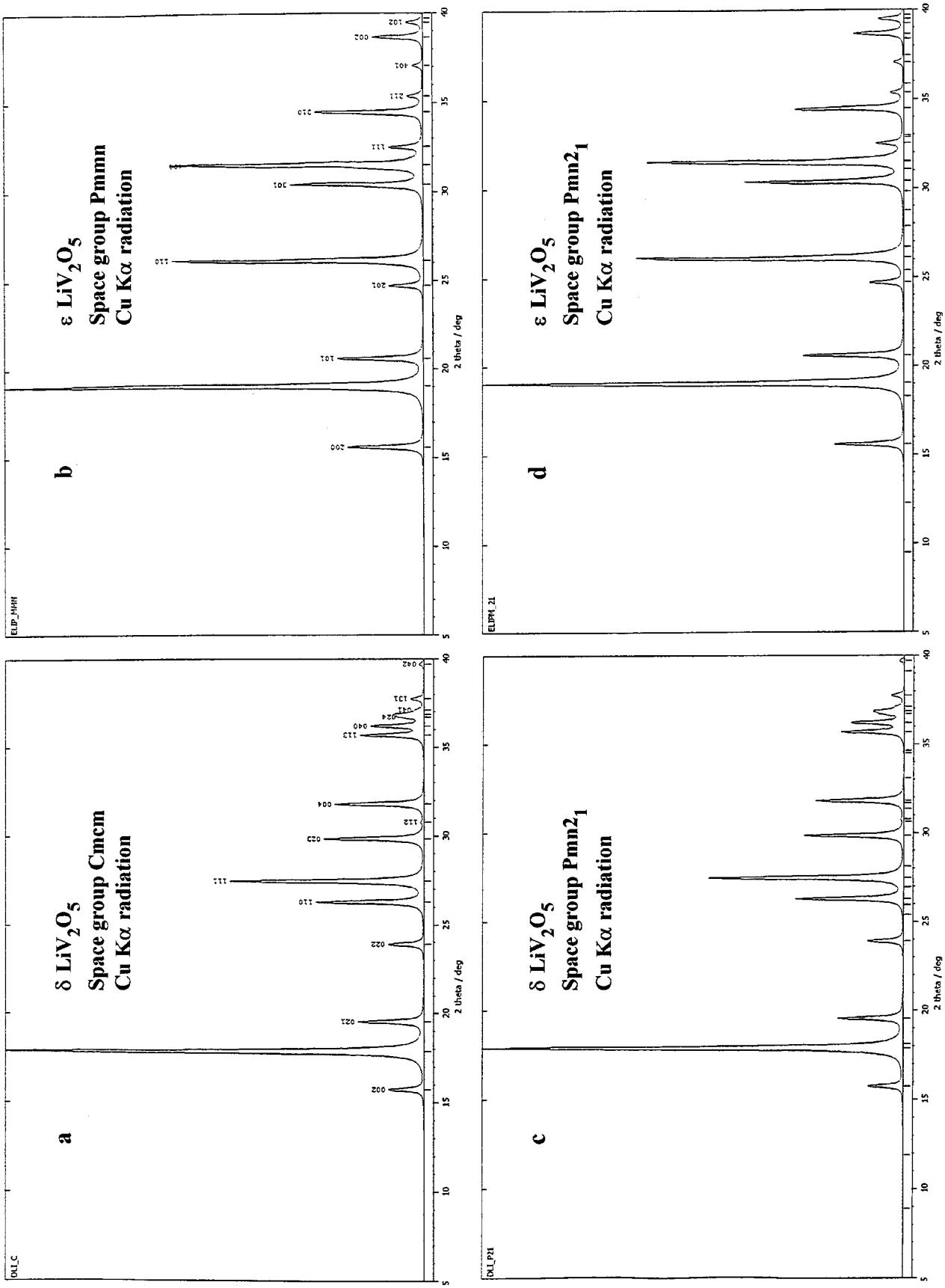

FIG. 2. Computed powder patterns of the δ and ε LiV_2O_5 phases (Cu$K\alpha$ radiation); (a) and (b) on the bases of the crystal structures of δ and ε phases, i.e., respective space groups *Cmcm* and *Pmnn*; (c) and (d) using the space group $Pmn2_1$ and a doubled *b* parameter for ε.

TABLE 1
Coordinates of the Atoms in the Two $[V_2O_5]_n$ Layers, I and II, and the Lithiums, Li1 and Li2, Allowing δ and ε LiV_2O_5 Phases to be Described in the $Pmn2_1$ Space Group

δ LiV_2O_5				ε LiV_2O_5			
Atoms	x	y	z	Atoms	x	y	z
Layer I				Layer I			
Li1	0	0.6492	0	Li1	0	0.6400	0
V1	0.3513	0.5443	0	V1	0.3499	0.5566	0
O11	0.3772	0.7029	0	O11	0.3721	0.7330	0
O21	0.1755	0.5051	0	O21	0.1740	0.5001	0
O31	0.5	0.4692	0	O31	0.5	0.4858	0
Layer II				Layer II			
Li2	0	0.1492	0.5	Li2	0	0.1400	0
V2	0.3513	0.0443	0.5	V2	0.3499	0.0566	0
O12	0.3772	0.2029	0.5	O12	0.3721	0.2330	0
O22	0.1755	0.0051	0.5	O22	0.1740	0.0010	0
O32	0.5	− 0.0308	0.5	O32	0.5	− 0.0142	0

The sequence of cell parameters is $a = 11.2479(4)$, $b = 9.9157(5)$, $c = 3.6047(2)$ Å. In this case the number of atomic positions must be doubled to describe both $[V_2O_5]_n$ layers alternately shifted along [001].

Atomic positions are as follows:

Layer I + Li1	Layer II + Li2
$x_1 = z_{\text{Cmcm}} - 1/4$	$x_2 = x_1$
$y_1 = y_{\text{Cmcm}} - 1/4$	$y_2 = y_1 + 1/2$
$z_1 = x_{\text{Cmcm}}$	$z_2 = z_1 + 1/2$

Throughout computation, the thermal parameters B (Å^2) have been locked to average values close to experimental ones.

All parameters are listed in Table 1. The powder patterns (Cu$K\alpha$ radiation) computed in the real *Cmcm* structure and simulated in $Pmn2_1$ are compared in Figs. 2a and 2c using the Kraus and Nolze program (13).

ε LiV_2O_5. This structure has already been determined in the space group *Pmmn* (12). To describe it in the space group $Pmn2_1$ (No. 31), the cell parameters have just been permuted and parameter b doubled: ($a = 11.3552(6)$, $b = 9.3096(3)$, $c = 3.5732(2)$ Å). Two identical layers are introduced whose atomic parameters are extrapolated from previous structure determinations (see Table 1):

Layer I + Li1	Layer II + Li2
$x_1 = x_{\text{Pmmn}} - 1/4$	$x_2 = x_1$
$y_1 = z/2_{\text{Pmmn}} + 1/2$	$y_2 = y_1 - 1/2$
$z_1 = y_{\text{Pmmn}} + 1/4$	$z_2 = z_1$

Figures 2b and 2d, computed for Cu$K\alpha$ radiation, show, like δ, the good agreement between ε powder patterns.

In Fig. 1 both structures are depicted along with the $Pmn2_1$ space group. By choosing the twofold helical axis along the [001] direction of the small parameter, rather than a perpendicular mirror plane, translation can easily be achieved step by step for this layer. We chose to set the z coordinates of the atoms describing layer I, as well as Li1, at $z = 0$; a shift of layer II was then computed along the [001] direction. If s stands for this shift, it is equal to $s = 0$ for the δ phase and 0.5 for the ε phase; thus the z coordinate of the atoms during the shift of layer II becomes $z = z_\delta - s$.

In the meantime, for each s value, the cell parameters have been adjusted, following the relations

$$a(s) = 0.2146s + 11.2479 \quad b(s) = -1.2122s + 9.9157$$
$$c(s) = -0.063s + 3.6047$$

and the atomic positions extrapolated from those in δ and ε. By way of example, a list of values for $s = 0.3$ is given in Table 2.

SIMULATION AND EVOLUTION OF THE XRD POWDER PATTERNS DURING THE $\delta \Leftrightarrow \varepsilon$ LiV_2O_5 PHASE TRANSITION

The recording wavelength of the powder patterns at ESRF was $\lambda = 0.64667$ Å. A simulation of both δ and ε in their most significant θ range, i.e., $5^\circ \leq \theta \leq 20^\circ$, is given in Figs. 3a and 3b.

Successive patterns have been computed to increase values of s in steps of $\Delta s = 0.02$ within the range $0 \leq s \leq 0.5$. The evolution of patterns versus s is given in Fig. 4 using

TABLE 2
Intermediate Cell Parameters and Atom Coordinates after a Shift $s = 0.3$ of Layer II

	a (Å)	b (Å)	c (Å)
	11.3123	9.5520	3.5858
Atom coordinates	x	y	z
Layer I			
Li1	0	0.64368	0
V1	0.35046	0.55168	0
O11	0.37414	0.72096	0
O21	0.17460	0.50210	0
O31	0.5	0.47916	0
Layer II			
Li2	0	0.14368	0.2
V2	0.35046	0.05168	0.2
O12	0.37414	0.22096	0.2
O22	0.17460	0.00264	0.2
O32	0.5	− 0.02084	0.2

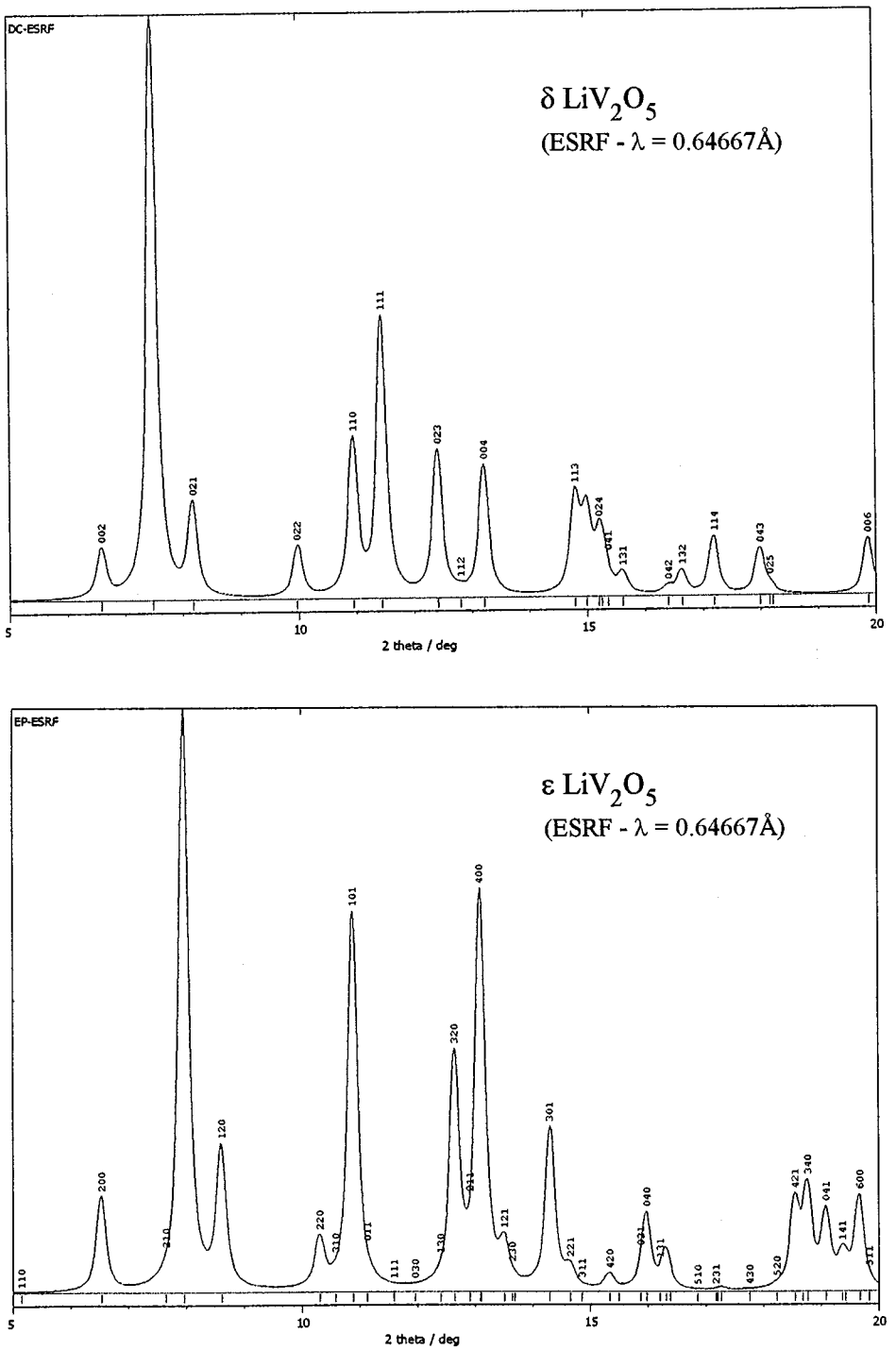

FIG. 3. Powder pattern simulation of the δ and ε phases; $5^\circ \leq \theta \leq 20^\circ$ range and $\lambda = 0.64667$ Å, a wavelength used at ESRF.

a program designed by Savariault (14). It is in good agreement with the experimental data obtained at ESRF when the δ LiV_2O_5 powder transforms under heating in the ε phase.

For this simulation, the $\varepsilon \Rightarrow \gamma$ transformation occurring between 175 and 220°C, has been added by introducing a progressive proportion of the γ phase to the detriment of ε (Fig. 4).

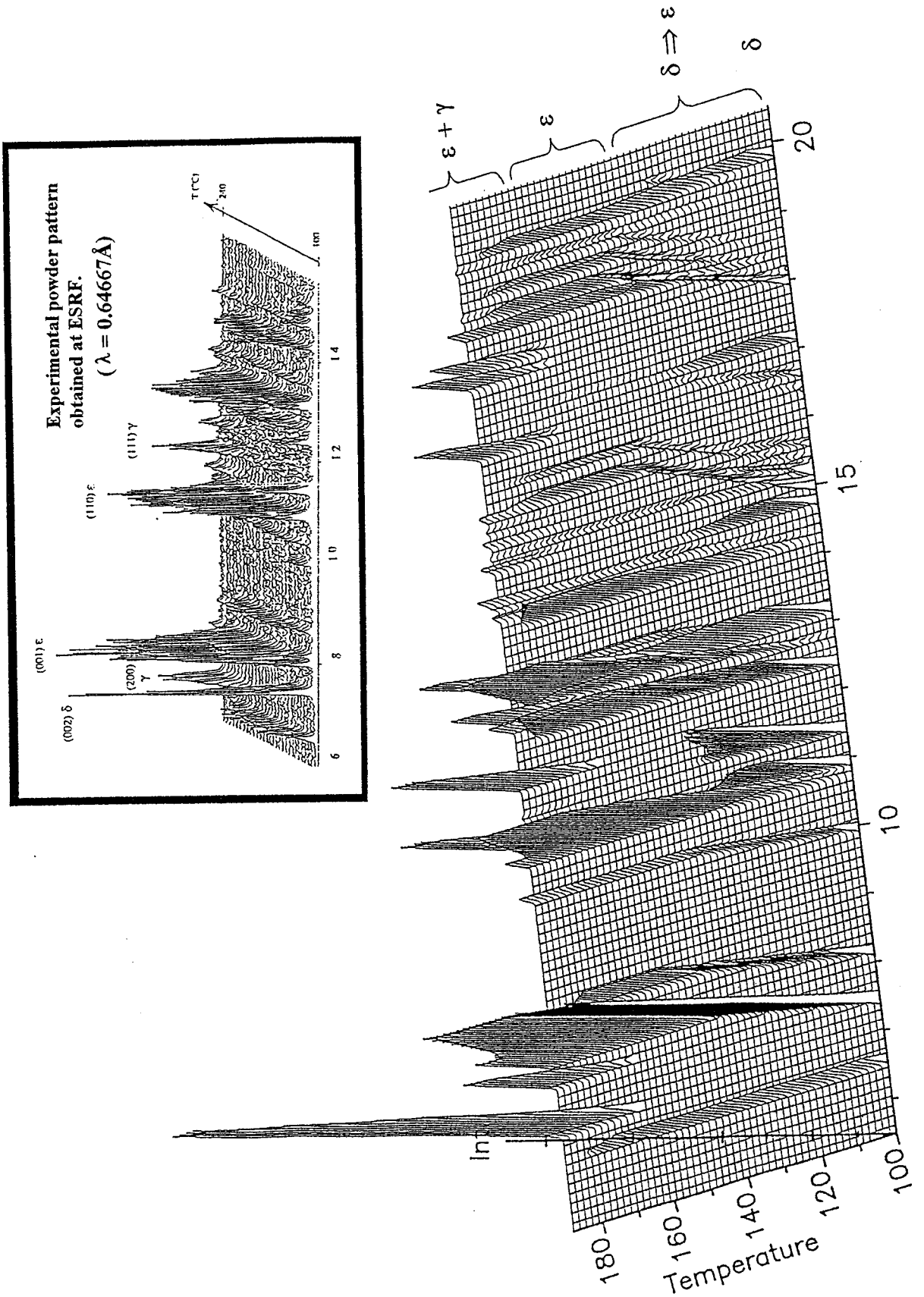

FIG. 4. Perspective view of the powder pattern evolution with temperature: — $\delta \Leftrightarrow \varepsilon$ phase transition, — ε phase stability domain, and – irreversible ε transformation into γ phase. Comparison with the experiment [1] shown in insert.

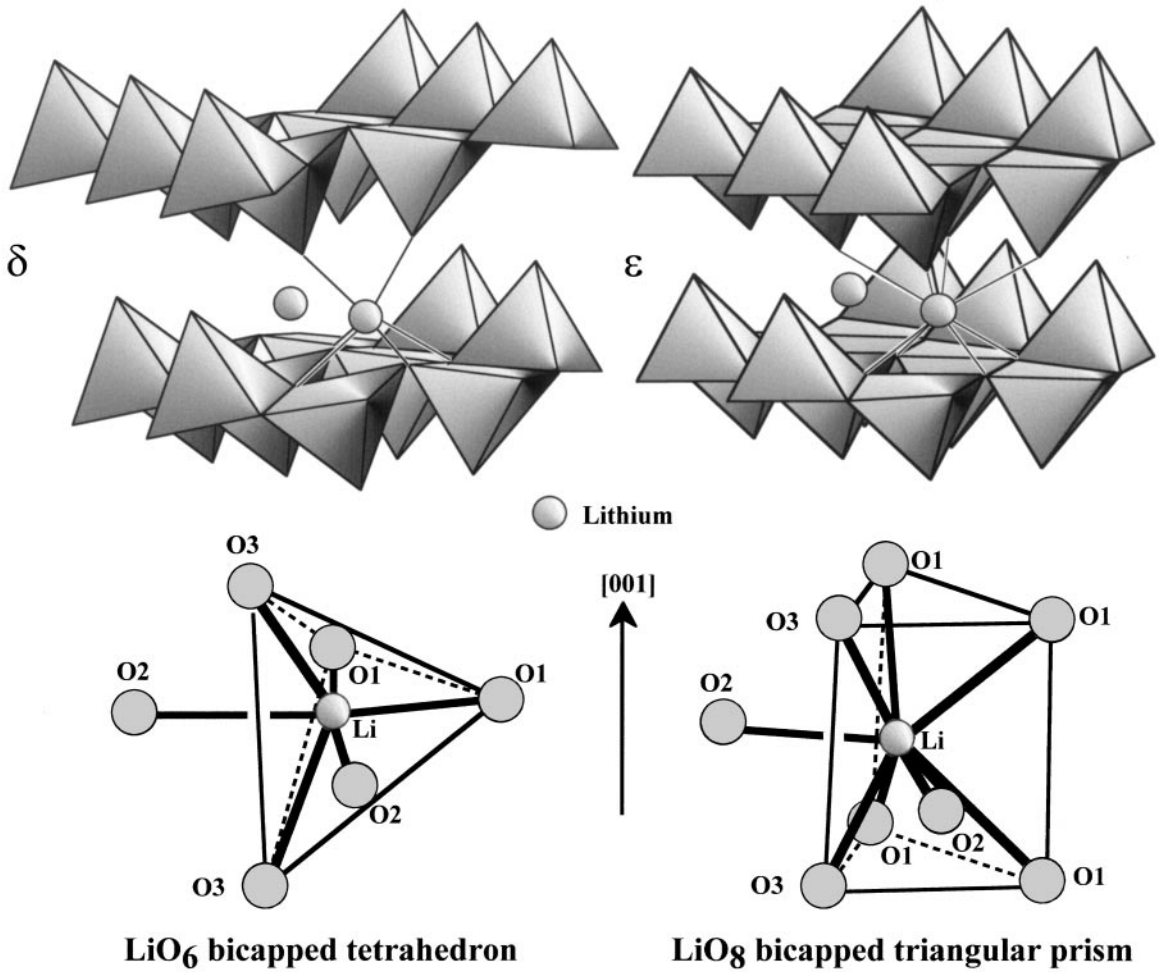

FIG. 5. Perspective view of two layers of both δ and ε structures allowing the lithium bonding to be observed and its coordination polyhedra after the $\delta \Leftrightarrow \varepsilon$ LiV_2O_5 phase transition.

DISCUSSION AND CONCLUSION

By using atomic modeling based on a crystallographic approach of both δ and ε, the structural dynamics of the transition has been thoroughly followed along with the resulting effects on the X-ray powder patterns. If the $[V_2O_5]_n$ layers move with a slight internal adjustment, the lithium atoms drastically alter their coordination scheme with oxygens from a bicapped tetrahedron to a bicapped triangular prism. This is shown in Fig. 5. During this displacement, lithium atoms are firmly bonded (four bonds: $2 \times$ Li–O3 = 2.026 Å, the two O3 oxygens (corner shared SP) repeated along c and $2 \times$ Li–O2 = 2.436 Å base oxygens O2 (edge shared SP) of the VO_5 square pyramids of the layer II; they evolve to $2 \times$ Li–O3 = 2.144 Å and $2 \times$ Li–O2 = 2.348 Å, respectively, after the transformation is achieved. The bond distances to layer I, $2 \times$ Li–O1 = 2.014 Å, are doubled but their length increase tremendously up to $4 \times$ Li–O1 = 2.634 Å. Lithiums come closer to layer I, the space becoming larger with the creation of the bicapped triangular prism site. This results in better packing of layers (the b parameter perpendicular to the $[V_2O_5]_n$ layers decreases by approximately 0.6 Å after the $\delta \Leftrightarrow \varepsilon$ LiV_2O_5 phase transition.

ACKNOWLEDGMENTS

This paper is dedicated to the Alexander von Humboldt-Stiftung. J. Galy thanks Prof. Dr. J. Strähle for his warm and fruitful welcome in his laboratory at the University of Tübingen (Germany).

REFERENCES

1. C. Satto, Ph. Sciau, E. Dooryhee, J. Galy, and P. Millet, *J. Solid State Chem.* **146,** 103 (1999).
2. J. Galy, J. Darriet, and P. Hagenmuller, *Rev. Chim. Miner.* **8,** 509 (1971).

3. J. Galy, *J. Solid State Chem.* **100,** 229 (1992).
4. P. Rozier, J. M. Savariault, and J. Galy, *Solid State Ionics* **98,** 133 (1997).
5. M. S. Witthingham, *J. Electrochem. Soc.* **123,** 315 (1976).
6. D. W. Murphy, P. A. Christian, F. J. Disalvo, and J. W. Wazczak, *Inorg. Chem.* **18,** 2800 (1979).
7. P. G. Dickens, S. J. French, A. T. Hight, and M. F. Pye, *Mater. Res. Bull.* **14,** 1295 (1979).
8. A. Carpy and J. Galy, *Acta Cryst. B* **31,** 1481 (1975).
9. P. Rozier, J. M. Savariault, J. Galy, C. Marichal, J. Hirschinger, and P. Granger, *Eur. J. Solid State Inorg. Chem.* **33,** 1 (1996).
10. J. M. Savariault, Ph. Sciau, and J. Galy, "Aperiodic'97, Proceeding of the International Conference on Aperiodic Crystals, France," 1997.
11. R. J. Cava, A. Santoro, D. W. Murphy, S. M. Zahurak, R. M. Fleming, P. Marsh, and R. S. Roth, *J. Solid State Chem.* **65,** 63 (1986).
12. P. Millet, C. Satto, Ph. Sciau, and J. Galy, *J. Solid State Chem.* **136,** 56 (1998).
13. W. Kraus and G. Nolze, PowderCell, FIMRST, Berlin, Germany, 1997.
14. J. M. Savariault, SAVATD program, CEMES, Toulouse, France, 1998.